Preprint Cambridge Centre for Computational Chemical Engineering ISSN 1473 – 4273

Skeletal chemical mechanism of high-temperature TEOS oxidation in hydrogen-oxygen environment.

Daniel Nurkowski [1], Philipp Buerger [1], Jethro Akroyd [1], Sebastian Mosbach [1], Markus Kraft [1,2]

released: 2 October 2015

[1] Department of Chemical Engineering
and Biotechnology
University of Cambridge
New Museums Site
Pembroke Street
Cambridge, CB2 3RA
United Kingdom
E-mail: mk306@cam.ac.uk

[2] School of Chemical
and Biomedical Engineering
Nanyang Technological University
62 Nanyang Drive
Singapore 637459

Preprint No. 160

Keywords: TEOS, mechanism reduction, DRG, *ab initio*

Edited by
Computational Modelling Group
Department of Chemical Engineering and Biotechnology
University of Cambridge
New Museums Site
Pembroke Street
Cambridge CB2 3RA
United Kingdom

Fax: + 44 (0)1223 334796
E-Mail: c4e@cam.ac.uk
World Wide Web: http://como.cheng.cam.ac.uk/

Highlights

- A skeletal mechanism describing TEOS oxidation in H_2:O_2 environment is proposed.
- A three-stage reduction is used to eliminate unimportant species and reactions.
- Rate parameters for the main TEOS decomposition pathways are refined using transition state theory.
- Energetics of the key reaction channels is improved using CBS-Q method.

Abstract

This paper improves the tetraethoxysilane (TEOS) oxidation mechanism proposed by Nurkowski et al. (*Proc. Comb. Inst.*, 35:2291-2298, 2015) by refining the rate parameters of the key reaction channels in the mechanism. A skeletal version of the mechanism is proposed for hydrogen-oxygen environment. The rates of ethylene-loss from (tetra-, tri-, di- and dimethyldi-) ethoxysilane are computed using transition state theory. The energetics of the main pathways are refined by performing detailed *ab initio* calculations using the CBS-Q technique. An analysis of ethanol formation via silicates is also performed resulting in the addition of 27 new silica species to the model. Thermodynamic properties for these species are calculated via the balanced reactions method. Reasonably good agreement between the improved model and available experimental data is observed. The subsequent elimination of unimportant species and reactions is achieved via a three-stage reduction procedure. The first and second stages involve the Direct Relation Graph with Error Propagation (DRGEP) method, whereas the third stage analyses rate of progress of each reaction. The investigated conditions are taken from the experimental studies of TEOS oxidation in oxygen-hydrogen flames. The final skeletal mechanism comprises 70 species and 457 reactions and retains good reproduction of the key model properties across the chosen operating conditions as compared to the full mechanism.

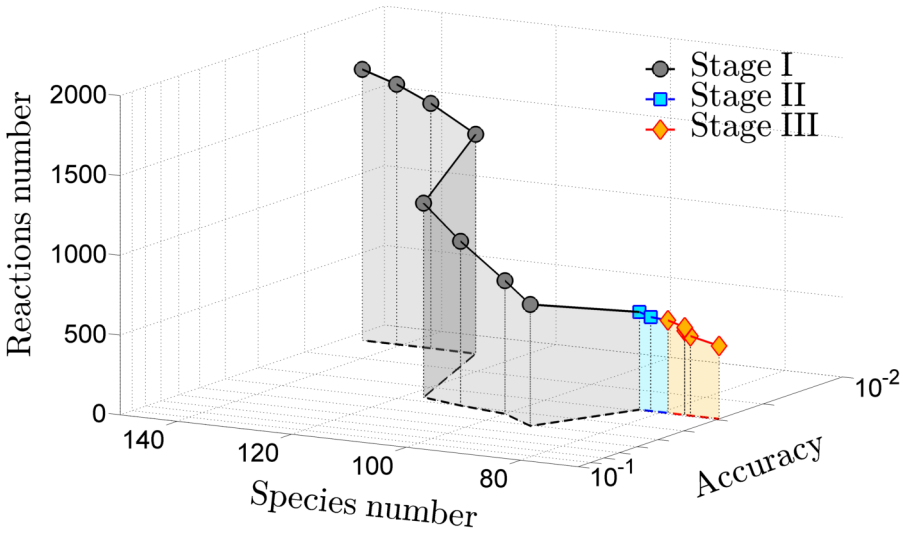

Contents

1 Introduction

The flame synthesis of silica nanoparticles from tetraethoxysilane (TEOS) is a well established process [2, 15, 48]. It offers continuous production of high purity particles without the need for subsequent steps like drying, calcination or milling in wet methods [18]. The use of TEOS as a precursor is of interest, because it is relatively cheap and a halide-free molecule thus making the production more cost-effective and eliminating the need for post-treatment of toxic by-products such as HCl.

Despite the industrial importance of TEOS, the knowledge of its gas-phase kinetics still remains incomplete. This poses difficulties in tuning the final product characteristics (e.g. particle size, surface area) because they are affected by the complex decomposition mechanism of TEOS. In order to tackle this problem a number of studies have been conducted.

The thermal stabilities of TEOS and tetramethyl orthosilicate (TMOS) have been investigated in a heated wall reactor [6]. Based on the rate of disappearance of the reactants, total decay rates were estimated and TMOS was found to be significantly more stable than TEOS. Abdali et al. [1] measured ignition delay times of TEOS in dry and humid air finding that the presence of moisture significantly lengthened the ignition delay. A detailed shock tube analysis of the thermal decomposition of TEOS was performed by Herzler et al. [16]. The experiments were carried at a temperature range of 1160-1285 K and pressure of 1.5-2 bar using highly diluted mixtures of TEOS in argon. Ethanol and ethylene were reported as the main detected products. Subsequently, an initial mechanism describing TEOS thermal decomposition was developed based on the observed product distributions, where a 1,2-elimination of ethylene and C−C bond cleavage in ethoxy groups were suggested to be the main decomposition pathways. Flame synthesis of silica nanoparticles from TEOS was investigated by Jang et al. [19, 20]. The effects of precursor concentration, residence time, and the flame temperature on the final particle characteristics were studied using oxygen-hydrogen diffusion flame. It was reported that an increase of each of the operating conditions caused the production of larger particles.

In addition to experimental studies, there have been number of computational studies to better understand the kinetics of TEOS decomposition. Ho and Melius [17] were the first to conduct *ab initio* calculations on Si−O−C−H system. They estimated thermodynamic properties of the selected silica species using the MP4 and MP2 levels of theory with bond additivity corrections (BAC). The silica species pool with complete thermochemical data was also extended by calculations performed by Kraft and co-workers [13, 41, 46, 49, 53]. They employed density functional theory (DFT) combined with isodesmic/isogyric reactions to more accurately predict the energetics of 180 species. Subsequently, equilibrium analysis was performed to reveal the most stable species and a heuristic gas-phase mechanism describing the thermal decomposition of TEOS was proposed [45].

A new approach to tackle TEOS gas-phase mechanism development was suggested by Nurkowski et al. [36], where possible reactions and their kinetic parameters were derived based on an analogy with ethanol decomposition [30]. The mechanism was analysed using flux and sensitivity studies, and the same pathways as suggested by Herzler et al. [16] were found to be important. A simple DFT method was used to estimate rate constant coefficients of the key silica and analogous ethanol channels. It was observed that the rate

coefficients in the silica and ethanol systems obtained at the same level of theory were similar (within a factor of 2). However, the comparison of the ethanol rates with the literature data suggested that more accurate methods would be beneficial.

Although TEOS has gained a lot of attention in the literature, the models developed so far remain incomplete. The difficulty in deriving a comprehensive gas-phase mechanism lies in the scarcity of appropriate experimental data. Therefore, the mechanisms published to date are either very small [9, 16], focusing just on bulk properties, or very large [36, 45] where a lot of parameters are estimated or extrapolated based on various analogies. One way of facilitating the development of a suitable gas-phase mechanism is to create a model that could be coupled with population balance or CFD codes [3, 31, 43, 44], thus enlarging the set of experimental data that can be used to inform the model. Such an approach must inevitably introduce a trade off between the size of the model and the amount of chemical information in it.

The main goal of this paper is to propose a skeletal version of the TEOS high-temperature oxidation mechanism in hydrogen-oxygen environment. We envisage this model to form a basis for future TEOS flame combustion modelling. However, before such a complex process can be simulated a proper understanding of the homogenous case is required first. To achieve this, a full model is first created that builds on the mechanism proposed by Nurkowski et al. [36] and incorporates rates improvements reported in the previous [37] and present work. The resulting mechanism is then used as the starting point for deriving a reduced mechanism. A three-stage reduction technique is employed. The first and second stages involve a DRGEP method, whereas the third stage analyses rate of progress of each reaction (ROP). A secondary goal is to improve the energetics of the main TEOS reaction pathways via detailed *ab initio* computations at CBS-Q level of theory for further mechanism development.

The structure of the paper is as follows. Section 2.1 provides a description of how the improved TEOS gas-phase mechanism was built. Sections 2.2 and 2.3 explains the details behind electronic structure and rate constants calculations respectively. Section 2.4 describes the mechanism reduction procedure, where a new method based on the ROP is presented. The results from the computations are reported in section 3. Final conclusions are drawn in section 4, various supplementary information is provided in section 5.

2 Theoretical background

2.1 Detailed mechanism

The current model builds on the detailed mechanism proposed by Nurkowski et al. [36]. In the cited work, all reactions and species were derived based on the analogy between the kinetics of the hydrocarbon branches (-OC_2H_5, -OCH_3, -OCH_2, -$OCH{=}CH_2$, -O, -OH, -OC_2H_4, and -$OCHCH_3$,) attached to the central silicon atom in TEOS and its intermediates and the kinetics of an ethanol. Main reaction channels can be classified into three main groups: 1) bond cleavage reactions (C−C and C−O bonds), 2) hydrogen abstraction and addition, and 3) elimination processes (C_2H_4, C_2H_3 and CH_2 removal). Initial estimate

Table 1: *Species short names.*

Chemical formula	Abbreviation used
$Si(OC_2H_5)_4$	TEOS
$Si(OH)(OC_2H_5)_3$	TREOS
$Si(OH)_2(OC_2H_5)_2$	DEOS
$Si(OH)_3(OC_2H_5)$	EOS
$Si(OCH_2)(OC_2H_5)_3$	TREMEOS
$Si(OH)(OCH_2)(OC_2H_5)_2$	DEMEOS
$Si(OH)_2(OCH_2)(OC_2H_5)$	EMEOS
$Si(OH)_3(OCH_2)$	MEOS
$Si(O)(OC_2H_5)_3$	TRE(O*)S
$Si(O)(OH)(OC_2H_5)_2$	DE(O*)S
$Si(O)(OH)_2(OC_2H_5)$	E(O*)S
$Si(CH_3)_2(OC_2H_5)_2$	DMDEOS
$Si(OH)(CH_3)_2(OC_2H_5)$	DMEOS
$Si(OCHCH_3)(OC_2H_5)_3$	TRE(*E)OS

of the rates parameters were mostly taken from the corresponding ethanol reactions from Marinov [30] and Park et al. [39] studies.

The reference mechanism for the reduction was then developed by taking the model described above and refining the kinetic parameters of its key channels, R1: 1,2-elimination of C_2H_4 and R2: C−C bond cleavage. Refinement of the first class of reactions was achieved by using more accurate rate constants for the C_2H_4-loss from TEOS, TREOS, DEOS and EOS (see Table 1) as a basis for the remaining analogous reactions. The first three channels were computed in this work, whereas the last one was taken from the calculation of Nurkowski et al. [37]. Refinement of the second class of reactions was achieved in the same way by using rate constant coefficient of the C−C bond cleavage in EOS from Nurkowski et al. [37]. The propagation of the improved rates throughout the analogous species in the mechanism was made under the assumption that species with the same number of hydrocarbon branches react at the same rate and that the rates linearly scale with the number of branches. Prior to the reduction, the rate constants of the ethylene-loss from TREOS and DEOS were further tuned within the error bars of the employed methods (see section 3.2 for further details). The resulting mechanism was then used as the starting point for the reduction.

2.2 Electronic structure calculations

The geometries and ro-vibrational properties of all stable species and transition states were obtained using the hybrid density functional B3LYP (Becke's three parameter non-local exchange functional [4] with the non-local correlation functional [23]) on the 6-311++G(d,p) basis set. The calculations were performed using the Gaussian09 software package [11].

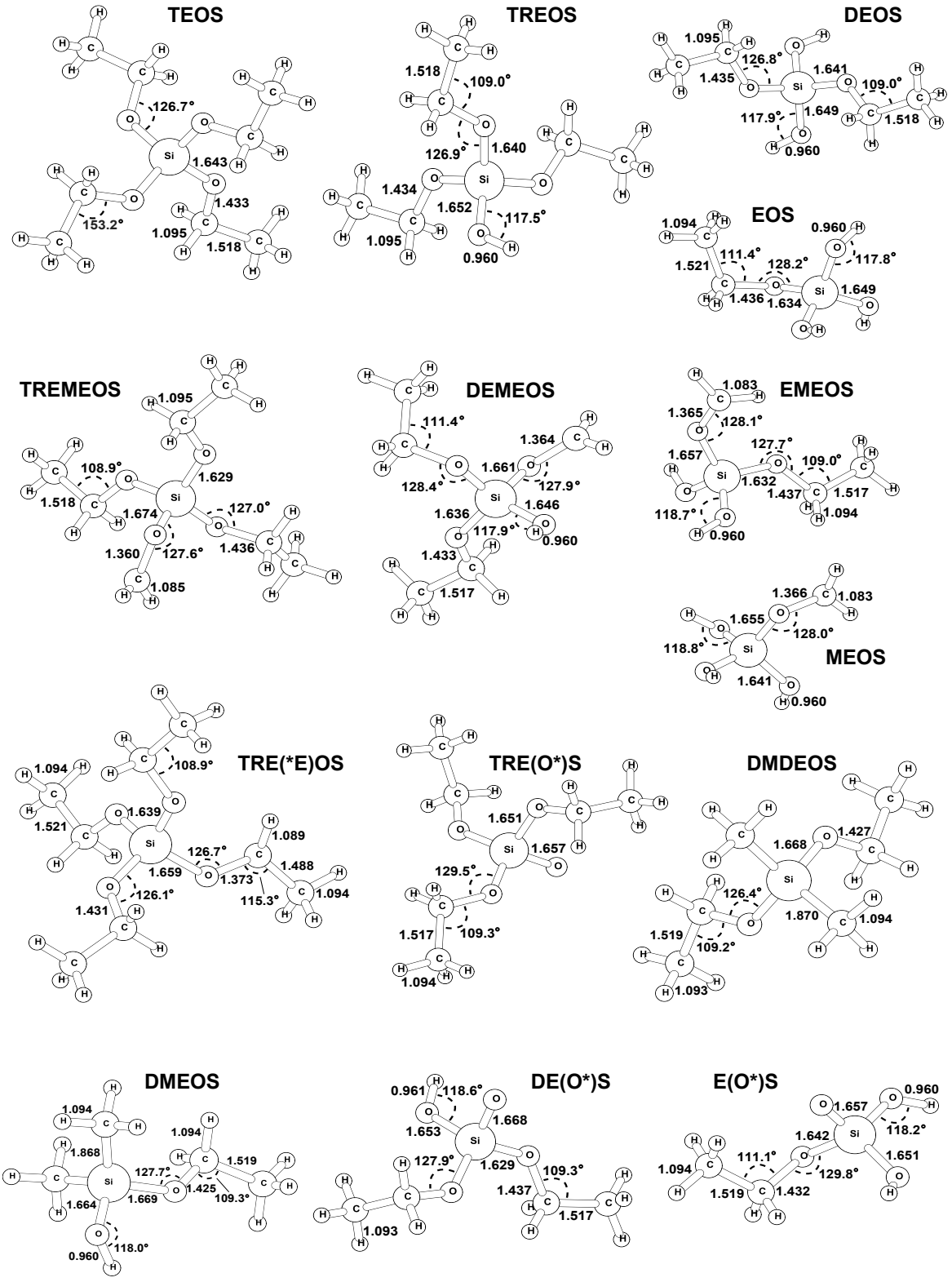

Figure 1: *Optimised ground state geometries of the species in Table 1 calculated at the B3LYP/6-311++G(d,p) level of theory. Units are deg and Å.*

The higher level energies of the investigated species were obtained by employing a complete basis set extrapolation method, CBS-Q, [32, 38] which is the most detailed technique used in this paper [10]. Additionally, Gaussian G2 computations [8] were performed for comparison. These computations are more expensive than CBS-Q in terms of the computational time and storage space requirements. Therefore, only molecules of a moderate size (less than 26 atoms) were considered.

2.3 Rate constant estimation

The reaction rate coefficients for the 1,2-elimination of ethylene were estimated using microcanonical RRKM method [21, 29, 42] employing barrier heights estimated at the CBS-Q level of theory. The density and number of states of the stable species and saddle points were evaluated according to the rigid-rotor harmonic-oscillator assumption. The identified transition states were further confirmed by running intrinsic reaction coordinate calculations (IRC) [12]. All the rate constants computations were performed using the Master Equation code [14].

2.4 Mechanism reduction

CFD models require small gas-phase mechanisms in order to be computationally feasible. In order to achieve this, the mechanism was reduced using a three-stage technique. The properties that were selected as the indicators of the accuracy of the reduced model were the mole fractions of the species lying on the main TEOS decomposition pathways: TEOS, TREOS, DEOS, EOS, $Si(OH)_4$, and C_2H_4, and the mole fractions of O_2, H_2 species in order to capture their chemistry. In addition, the temperature and concentrations of OH and H radicals were used when assessing how far the mechanism could be reduced.

Reduction conditions. The conditions that the reduced mechanism was built for are taken from the experimental studies of Herzler and Jang et al. [16, 19, 20]. They span

Table 2: *Process conditions used to generate reduced model.*[a]

Case	x_{TEOS}	x_{Ar}	x_{O_2}	x_{H_2}	x_{N_2}	T	P	PSR mode	Ref.
1-9	0.04	99.96	0.0	0.0	0.0	1140-1300	2	const P,T	[16]
10-12	0.13	15.26	32.46	8.32	43.83	1200-1600	1	const P	[19]
13-15								const P,T	
16-18	3.18	14.79	31.47	8.07	42.49	1200-1600	1	const P	[19]
19-21								const P,T	
22-24	0.07	10.34	31.53	17.23	40.83	1200-1600	1	const P	[20]
25-27								const P,T	
28-30	0.29	10.32	31.46	17.19	40.74	1200-1600	1	const P	[20]
31-33								const P,T	

[a] Units of T and P are Kelvins and atmospheres, respectively.

various cases, presented in Table 2, ranging from TEOS thermal decomposition in argon to its oxidation in hydrogen-oxygen flames. Simulations were performed using a perfectly stirred reactor (PSR) models, where either pressure or pressure and temperature were held constant. For cases 1-9 in Table 2 simulations' time and temperature increment were equal to 0.5 ms and 20 K respectively. For cases 10-33 the simulations' times were adjusted so that TEOS was entirely consumed and temperature increment was equal to 200 K. The choice of the PSR model was motivated by the ability to quickly generate a large set of diverse sample points. The simulation results then served as inputs to the mechanism reduction scheme.

Reduction stages. The idea of using more than one reduction stage was proposed by Lu and Law [28], where they showed that it facilitates the reduction of large mechanisms. In this paper the mechanism is reduced using three reduction stages, performed sequentially. The first and second stage involve a DRGEP method, while the third stage analyses rates of progress of the reactions (ROP). Details of the DRGEP method can be found in many publications [27, 34, 40], therefore only brief explanation is presented.

The DRGEP stages prioritise species in the mechanism according to their coupling strength with a set of target species predefined by the user. The skeletal model is then built by removing the least important species one after another until a user-specified error tolerance on each of the reduction targets is reached. This procedure is repeated for all selected conditions and the resulting mechanism contains a union of species and pathways from each studied condition. However, in many cases, the resulting mechanism contains a number of reactions that are very slow.

The third stage of the reduction seeks to resolve this problem by introducing a method that ranks the reactions in the mechanism. Several such techniques have been proposed in the past, where reactions are prioritized based on flow analysis of the key elements [35, 50], sensitivity analysis of the key model parameters [51] or on the DRG-based reaction couplings with the targets [40]. Further details on these methods can also be found in the work of Løvås et al. [24–26]. In this paper, however, a simple analysis of the reactions rates of progress (ROP) combined with an actual error estimation is used. This is similar to a classical flux reduction method [33, 52]. The idea is to detect very slow reactions and estimate the errors on the key model parameters after removing these channels. Because there are multiple simulation cases and the reactions rates of progress are time-resolved quantities, the following importance indicator is proposed:

$$\Omega_i = \frac{\sum\limits_{\text{cases } j} \int_0^{t_{\text{end}}} |\omega_{ij}(t)| \mathrm{d}t}{\sum\limits_{\text{reactions } i} \sum\limits_{\text{cases } j} \int_0^{t_{\text{end}}} |\omega_{ij}(t)| \mathrm{d}t} \tag{1}$$

where $\omega_{ij}(t)$ is a rate of progress of reaction i in case j at the time point t.

Reduction errors. After each reduction stage, the errors with respect to the reference mechanism were calculated for the chosen set of targets across all the cases. The following metric was used to calculate the global relative error for each simulation case:

$$\varepsilon_{kj} = \frac{\int_0^{t_{\text{end}}} |\Phi_{kj}^R(t) - \Phi_{kj}^F(t)| \mathrm{d}t}{\int_0^{t_{\text{end}}} |\Phi_{kj}^R(t)| + |\Phi_{kj}^F(t)| \mathrm{d}t} \tag{2}$$

where ε_{kj} is the normalized error in case j for target k, and $\Phi_{kj}^R(t)$, $\Phi_{kj}^F(t)$ are the values of chosen targets in the reduced and full mechanism at the time point t respectively.

Finally a root mean square error (RMS) was calculated as a final error indicator across all the cases,

$$\bar{\varepsilon}_k = \sqrt{\frac{1}{N} \sum_{\text{cases } j} \varepsilon_{kj}^2} \tag{3}$$

where N is the number of simulations.

3 Results and discussion

3.1 Potential energy surface

Table 3 presents the energetics of the main TEOS decomposition channels obtained at various levels of theory. The reaction barriers, enthalpies at 0 and 298 K ($E^{\ddagger}$, ΔH_r^0 and ΔH_r^{298}) are provided where applicable. In addition, the energetics of reactions producing ethanol via silicates are reported. The accuracy of the computed energetics is somewhat difficult to assess since neither experimental data nor more detailed computations other than the ones in this paper exist. Therefore, it was decided to report the analogous ethanol reactions for which good quality data are available [47]. The results from systematic BAC-MP4 and BAC-MP2 computations performed by Ho and Melius [17] are also included. Although the methods used by Ho and Melius [17] are on average less accurate than CBS-Q [7] they can still be used for a consistency check. The results for each reaction channel are discussed.

1,2-elimination of C_2H_4. The reactions occur via a tight 4-center transition state. The first four channels are the main decomposition pathways of TEOS. The decomposition of DMDEOS was added for comparison with the current study and literature. It can be seen that the barriers of the silica reactions obtained at CBS-Q level of theory are similar to each other, with a maximum difference of 2.4 kcal/mol. Additionally, each replacement of the hydroxy group by an ethoxy branch decreases the barrier height by 0.3-0.9 kcal/mol. The same trend can be observed from the available data at the G2 level of theory.

This finding motivates the approach taken in developing the mechanism in the present work, where four different rate constants were used for C_2H_4-loss depending on the number of ethoxy branches. These rates are then propagated throughout the mechanism for analogous species. An assumed analogy between species having the same number of ethoxy branches is consistent with the results obtained for DEOS and DMDEOS and experimental observations [16]. The computed barrier height of C_2H_4-elimination from DMDEOS is only 0.2 kcal/mol higher than for their silanol analogue DEOS.

Table 3: *Energetics of the main decomposition TEOS channels and selected ethanol reactions.*[a]

Reactions		B3LYP[b]	G2[c]	CBS-Q[d]	Lit.
1,2-elimination of C_2H_4					
$TEOS \rightarrow TREOS + C_2H_4$	$E^{\ddagger}$	58.4		62.5	
	ΔH_r^0	8.9		13.3	
	ΔH_r^{298}	9.6		13.9	10.5[e]
$TREOS \rightarrow DEOS + C_2H_4$	$E^{\ddagger}$	58.4		62.8	
	ΔH_r^0	9.1		13.1	
	ΔH_r^{298}	9.7		13.7	11.8[e]
$DEOS \rightarrow EOS + C_2H_4$	$E^{\ddagger}$	58.2	63.2	63.7	
	ΔH_r^0	9.6	13.3	13.4	
	ΔH_r^{298}	10.2	13.8	14.0	11.6[e]
$EOS \rightarrow Si(OH)_4 + C_2H_4$	$E^{\ddagger}$	57.6	64.1[f]	64.0	70.7[e]
	ΔH_r^0	8.8	12.6[f]	12.9	
	ΔH_r^{298}	9.5	13.4[f]	13.6	12.0[e]
$DMDEOS \rightarrow DMEOS + C_2H_4$	$E^{\ddagger}$	59.3	64.6	63.9	
	ΔH_r^0	9.9	14.0	12.9	
	ΔH_r^{298}	10.6	14.9	13.7	
$C_2H_5OH \rightarrow H_2O + C_2H_4$	$E^{\ddagger}$	61.7	66.8	66.3	66.0[g]
	ΔH_r^0	8.4	10.3	9.9	9.7[g]
	ΔH_r^{298}	9.4	11.9	11.5	
C-C bond cleavage					
$TEOS \rightarrow TREMEOS + CH_3$	ΔH_r^0	80.2		88.0	
	ΔH_r^{298}	82.0		89.9	
$TREOS \rightarrow DEMEOS + CH_3$	ΔH_r^0	79.8		87.5	
	ΔH_r^{298}	81.5		89.3	
$DEOS \rightarrow EMEOS + CH_3$	ΔH_r^0	79.6	88.8	87.9	
	ΔH_r^{298}	81.4	90.6	89.7	
$EOS \rightarrow MEOS + CH_3$	ΔH_r^0	79.3	88.4[f]	87.6	
	ΔH_r^{298}	81.2	90.4[f]	89.6	89.4[e]
$C_2H_5OH \rightarrow CH_2OH + CH_3$	ΔH_r^0	78.0	86.5[f]	85.4	85.6[g]
	ΔH_r^{298}	79.4	88.5[f]	87.5	
O-C bond cleavage					
$TEOS \rightarrow TRE(O^*)S + C_2H_5$	ΔH_r^0	86.6		100.5	
	ΔH_r^{298}	87.6		101.5	100.9[e]
$TREOS \rightarrow DE(O^*)S + C_2H_5$	ΔH_r^0	87.6		101.3	
	ΔH_r^{298}	88.6		102.2	102.2[e]
$DEOS \rightarrow E(O^*)S + C_2H_5$	ΔH_r^0	88.4	101.4	102.2	

Reactions		B3LYP[b]	G2[c]	CBS-Q[d]	Lit.
	ΔH_r^{298}	89.6	102.4	103.4	
EOS $\rightarrow$ $Si(O)(OH)_3 + C_2H_5$	ΔH_r^0	87.7	101.2	101.0	
	ΔH_r^{298}	88.9	102.2	102.1	102.2[e]
$C_2H_5OH \rightarrow C_2H_5 + OH$	ΔH_r^0	84.9	94.4	93.1	92.6[g]
	ΔH_r^{298}	86.2	96.2	95.0	
Ethanol producing channels					
Six-centered molecular decomposition					
TEOS $\rightarrow$ $O{=}Si(OC_2H_5)_2 + C_2H_4$	ΔH_r^0	68.5		83.8	
$+ C_2H_5OH$	ΔH_r^{298}	69.2		84.5	80.2[e]
TREOS $\rightarrow$ $O{=}Si(OH)(OC_2H_5)$	ΔH_r^0	69.6		84.2	
$+ C_2H_4 + C_2H_5OH$	ΔH_r^{298}	70.2		84.7	82.1[e]
DEOS $\rightarrow$ $O{=}Si(OH)_2 + C_2H_4$	ΔH_r^0	70.8	81.2	84.6	
$+ C_2H_5OH$	ΔH_r^{298}	71.4	81.7	85.1	82.7[e]
Four-centered molecular decomposition					
TREOS $\rightarrow$ $O{=}Si(OC_2H_5)_2$	ΔH_r^0	59.6		70.6	
$+ C_2H_5OH$	ΔH_r^{298}	59.6		70.6	69.7[e]
DEOS $\rightarrow$ $O{=}Si(OH)(OC_2H_5)$	ΔH_r^0	60.5	67.8	71.1	
$+ C_2H_5OH$	ΔH_r^{298}	60.5	67.7	71.0	70.3[e]
EOS $\rightarrow$ $O{=}Si(OH)_2 + C_2H_5OH$	ΔH_r^0	61.2	67.9	71.2	
	ΔH_r^{298}	61.2	67.9	71.2	71.1[e]
Through diethyl ether formation					
TEOS $\rightarrow$ $O{=}Si(OC_2H_5)_2$	ΔH_r^0	55.5		66.8	
$+ C_2H_5OC_2H_5$	ΔH_r^{298}	55.3		66.6	64.7[e]
TREOS $\rightarrow$ $O{=}Si(OH)(OC_2H_5)$	ΔH_r^0	56.5		67.1	
$+ C_2H_5OC_2H_5$	ΔH_r^{298}	56.3		66.8	66.6[e]
DEOS $\rightarrow$ $O{=}Si(OH)_2$	ΔH_r^0	57.8	64.6	67.5	
$+ C_2H_5OC_2H_5$	ΔH_r^{298}	57.5	64.2	67.2	67.2[e]

[a] Zero point corrections are included throughout. Units are kcal mol^{-1}.

[b] B3LYP computations for the 6-311++G(d,p) basis set.

[c] Gaussian G2 method estimating RCCSD(T)/6-311+G(3df,2p) energies.

[d] Complete basis set extrapolation [32, 38].

[e] BAC-MP4 and BAC-MP2 data from [17].

[f] G2 data from Nurkowski et al. [37].

[g] QCISD(T)/CBS data from Sivaramakrishnan et al. [47].

The results obtained for ethanol highlight the benefit from increasing the level of theory. Our CBS-Q predictions of the $E^{\ddagger}$ and ΔH_r^0 are only 0.3 and 0.2 kcal/mol higher than

the very detailed computations of Sivaramakrishnan et al. [47] using the QCISD(T)/CBS method. It can be seen that performance of the DFT method at the B3LYP level of theory is much worse given the 4.6 and 1.5 kcal/mol differences in $E^{\ddagger}$ and ΔH_r^0 respectively to the reference data [47]. It is therefore believed that the chosen CBS-Q method is much more suitable.

The reaction enthalpies at 298 K reported by Ho and Melius [17] are 1.6-3.4 kcal/mol higher than the current CBS-Q results, which is well within the error bounds of their methods (3-9 kcal/mol). Additionally, the estimated activation energy of EOS is 6.7 kcal/mol lower than the Ho and Melius [17] value. However, as it was stated in their paper, the method they used to compute the barrier was most likely not adequate and has large uncertainty.

C−C bond cleavage. The calculated C−C bond dissociation energies at 0 and 298 K for the main silica species are within 0.6 kcal/mol difference with each other at CBS-Q level of theory. For this reason only one reaction for C−C bond breakage was used when developing the mechanism in this work. The ΔH_r^{298} reported by Ho and Melius [17] for EOS is also consistent with these findings.

The analysis of the ethanol data again demonstrates the accuracy of the CBS-Q technique. Our estimation of ΔH_r^0 is only 0.2 kcal/mol different from the detailed computations of Sivaramakrishnan et al. [47].

O−C bond cleavage. The obtained energies are very similar among silica species. Very good agreement with the computations of Ho and Melius [17] and Sivaramakrishnan et al. [47] can be seen where the reaction enthalpies at 298 K for silica species and ethanol are within 0.6 kcal/mol and 0.5 kcal/mol error respectively.

Ethanol formation pathways. Three different types of reaction that could account for the ethanol production were studied (see Table 3). The first family of reactions is a six-centered molecular decomposition proposed by Chu et al. [6]. These channels lead to the formation of equal amounts of silicates, O=Si(X)(Y), ethylene and ethanol. The second type is a four-centered molecular decomposition. In this case, ethanol is produced via recombination of hydroxy and ethoxy groups. A third option is the indirect formation of ethanol, via diethyl ether intermediate, where the ether decomposes into ethanol and ethylene in a secondary step [22]. Only reactions enthalpies at 0 and 298 K were calculated.

The results obtained for the six-centered molecular decomposition reveal that these channels have the highest endothermicities across all studied reactions ($\Delta H_r^0 > 80$ kcal/mol at the CBS-Q level of theory). Similar values were reported by Ho and Melius [17], where the discrepancies in ΔH_r^{298} are within 2.4-4.3 kcal/mol. A trend can also be noticed in that each replacement of -OC_2H_5 by -OH group in the reactant increases the reaction's endothermicity by 0.4 kcal/mol.

The formation of ethanol via secondary processes involving silanols (reactants with -OH groups) proceeds via reactions with slightly lower endothermicites than the previous channels ($\Delta H_r^0 \sim 70$ kcal/mol at the CBS-Q level of theory). Again, reaction enthalpies moderately increase with the number of hydroxy groups. Good agreement with the literature data can also be seen.

Production of ethanol via a diethyl ether intermediate has the smallest endothermicity

among all studied reactions ($\Delta H_r^0 \sim 67$ kcal/mol at CBS-Q level). As in previous cases, its value slightly increases (0.3-0.4 kcal/mol) with the number of hydroxy groups. The Ho and Melius [17] calculations are within 1.9 kcal/mol of our data.

The extent to which these pathways are able to explain the experimentally observed production of ethanol is considered in more detail in section 3.2.

3.2 Refined mechanism

Reference data. The experimental measurements of Herzler et al. [16] were used to assess the quality of the refined TEOS mechanism. The experiments were modelled by running a series of batch reactor simulations at different temperatures. The initial concentrations of reactants, pressure and simulation time were set to 420 ppm TEOS in argon, 2 bara and 500 μs respectively.

Rates improvement. Table 4 shows the rate coefficients of the most important TEOS pathways that were used to built the refined mechanism. The ethylene elimination from TEOS, TREOS and DEOS come from computations in this work, while the ethylene-loss and C−C bond cleavage in EOS were obtained from Nurkowski et al. [37]. Additionally, the rate constant coefficient of the ethylene loss from DMDEOS was computed for comparison purposes and as a further accuracy check against the available literature data. Optimised geometries of found transition states and stable species are presented on Figures 1 and 2.

Figure 3 depicts the estimated total decomposition rate constants of TEOS and DMDEOS compared with the measurements from Herzler et al. [16] and the DFT-based computations of Nurkowski et al. [36]. The total decay rate of TEOS in this work was calculated from the time-concentration profiles simulated using the refined mechanism. This approach automatically includes all the reactions in a given model that affect the TEOS kinetics. However, it was found that exactly the same rates are obtained by simply summing the main TEOS channels: elimination of C_2H_4, C−C and O−C bond cleavage. This indicates that any other channels (e.g. reverse reactions) other than those listed above constitute only very minor contributions to the TEOS decomposition at the given conditions. The DMDEOS and TEOS total decomposition rates from Nurkowski et al. [36] were also obtained by the summation of the main channels. It can be seen from Figure 3 that the decomposition rates computed in this work are in very good agreement with the experimental measurements. The TEOS results maximally differ only by 20%, while any discrepancies in the DMDEOS data are only noticeable at low temperatures. Overall, it is expected that the accuracy of the estimated rates, given the size of the molecular system, is within a factor of 2. Furthermore, contrasting these rates with the previous DFT-based estimates [36] explains why increasing the level of theory was beneficial. The old data [36] are within a factor of two with the current results at low temperatures ($T < 1200$ K) whereas at high temperatures the difference increases reaching as much as a factor of 7 at 1280 K.

Ethylene yield reproduction. Figure 4 compares the yield of ethylene measured by Herzler et al. [16] with the current modelling predictions. It can be seen that compared to our

Table 4: *High-pressure limited rate constant coefficients for important TEOS channels in modified Arrhenius form.*[a]

Reactions	$k = AT^n \exp(E_0/T)$	Ref.
Reactions used in deriving improved TEOS model		
1,2-elimination of C_2H_4		
TEOS $\rightarrow$ TREOS + C_2H_4	$k_{1a} = 4.832 \times 10^{11} T^{0.824} \exp(-31814/T)$	present
TREOS $\rightarrow$ DEOS + C_2H_4	$k_{1b} = 5.244 \times 10^{11} T^{0.823} \exp(-32004/T)$	present
DEOS $\rightarrow$ EOS + C_2H_4	$k_{1c} = 4.134 \times 10^{11} T^{0.810} \exp(-32467/T)$	present
EOS $\rightarrow$ $Si(OH)_4$ + C_2H_4	$k_{1d} = 2.527 \times 10^{7} T^{1.875} \exp(-30969/T)$	[37]
C−C bond cleavage		
TEOS $\rightarrow$ TREMEOS + CH_3	$k_{2a} = 4k_{2d}$	approx.
TREOS $\rightarrow$ DEMEOS + CH_3	$k_{2b} = 3k_{2d}$	approx.
DEOS $\rightarrow$ EMEOS + CH_3	$k_{2c} = 2k_{2d}$	approx.
EOS $\rightarrow$ MEOS + CH_3	$k_{2d} = 1.351 \times 10^{24} T^{-2.114} \exp(-46263/T)$	[37]
Additionally studied reaction		
1,2-elimination of C_2H_4 from DMDEOS		
DMDEOS $\rightarrow$ DMEOS + C_2H_4	$k_{1e} = 5.316 \times 10^{11} T^{0.834} \exp(-32600/T)$	present

[a] Units are seconds, and kelvins.

previous study [36] the agreement with the experimental data is slightly worse. The yield is under-predicted by 20-30% at temperatures above 1220 K. The observed discrepancies are the combined effect of recalculating the barrier heights of the important reactions contributing to the ethylene release (previously underestimated by the DFT method, see Table 3), differences in experimental and modelling parameters (e.g. residence time) and the effect of any missing channels (e.g. ethanol-producing reactions). A flux analysis was performed in order to assess the potential cause of the ethylene under-prediction in the current model.

Parameter tuning. Figure 5 shows the main integrated fluxes of carbon at 1260 K. It can be seen that the main contributions to the ethylene production from the silica species come from the decomposition of TEOS, TREOS and DEOS. These are the first three reactions in Table 4. It was decided to check how much the ethylene yield can be improved by varying the rate constant coefficients of these reactions within the error bars of the calculation method (about a factor of 2). Since the total TEOS decomposition rate constant agrees very well with the experimental data, only the TREOS and DEOS rates were varied.

Figure 4 shows the outcome of the parameter tuning, where the activation barrier height of ethylene loss from TREOS and DEOS were reduced by 2 kcal/mol. Given the size of the studied molecular system, it is believed that this is the maximum uncertainty of the CBS-Q computations (especially for the saddle points), which in turn gives an uncertainty

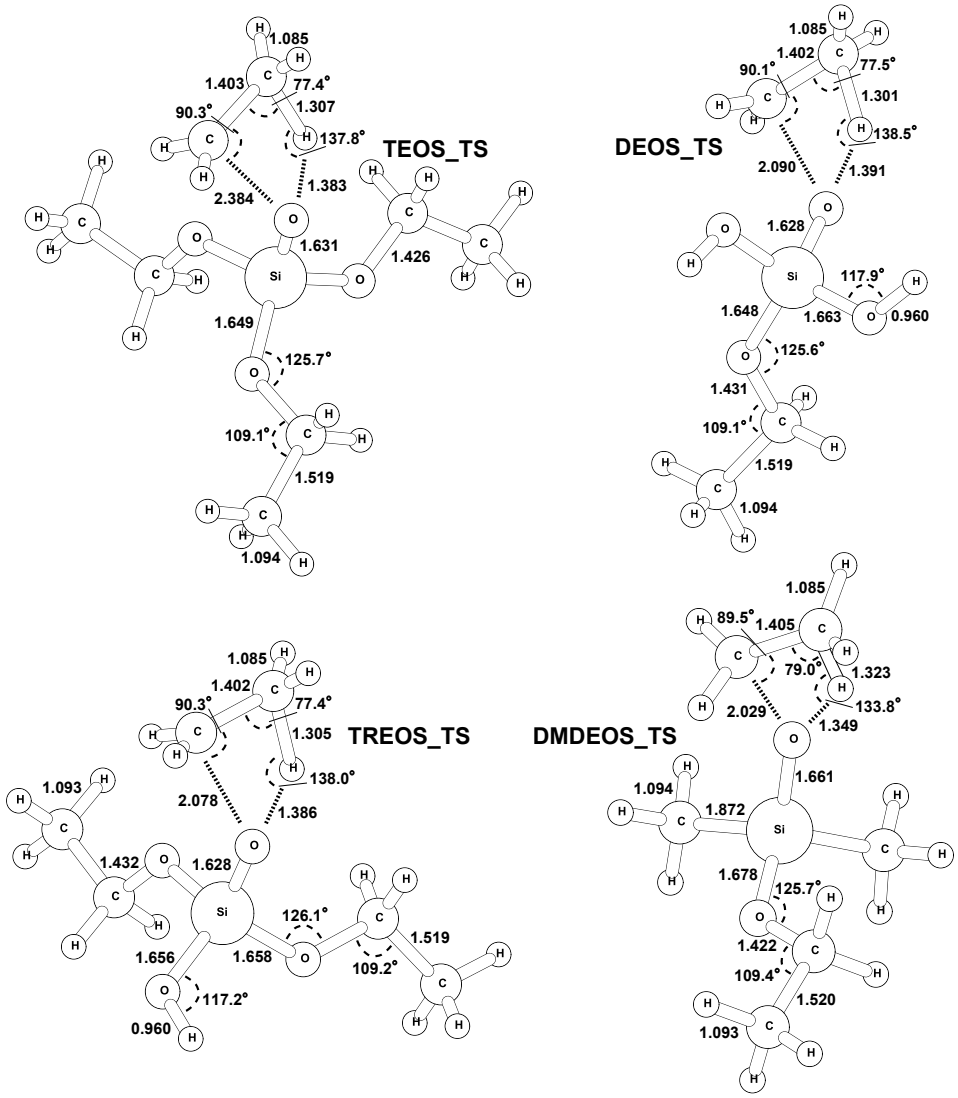

Figure 2: *Optimised geometries of the transition states for ethylene-loss from TEOS, TREOS, DEOS and DMDEOS calculated at the B3LYP/6-311++G(d,p) level of theory. Units are deg and Å.*

of a factor of 2 in the resulting rate constant coefficients. As shown in Figure 4, the adjustment of the barrier heights improves the agreement of the ethylene predictions versus the experiment. This adjustment is consistent with the findings of Herzler et al. [16], where rates of ethylene-loss from TREOS, DEOS and EOS in their model were increased to be somewhat larger than the initially estimated values in order to achieve agreement with the measured data.

Ethanol yield reproduction. An attempt has also been made to check whether or not it is possible to reproduce the experimental data for ethanol production [16]. A very similar approach was taken to the one presented by Herzler et al. [16]. The channels listed in Table 3 for ethanol production were incorporated into the current TEOS mechanism. The incorporation was performed in a systematic way, such that these reactions were added

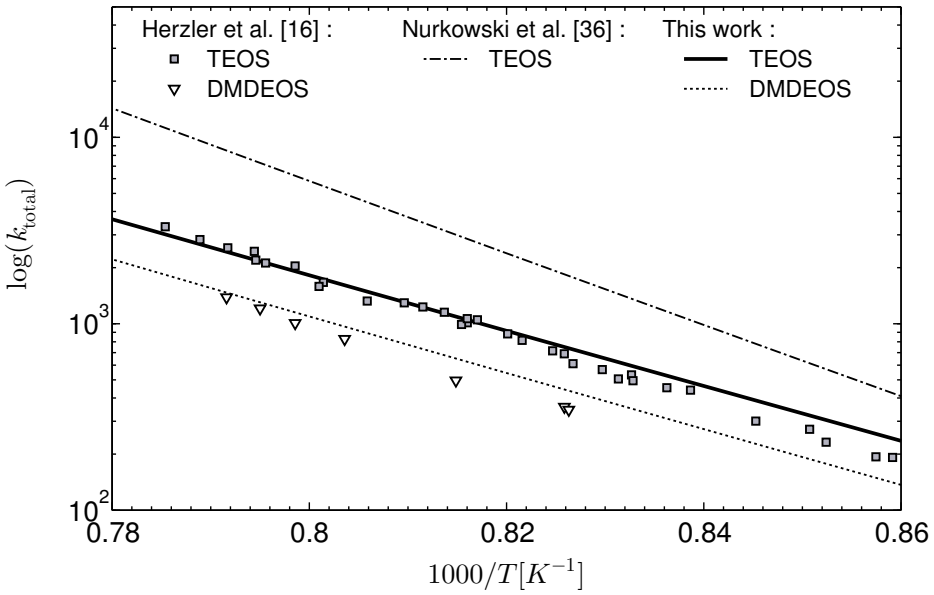

Figure 3: *Arrhenius plot of the computed total decomposition rate constants of TEOS and DMDEOS. Experimental measurements from Herzler et al. [16] and DFT-based results from Nurkowski et al. [36] are included for comparison.*

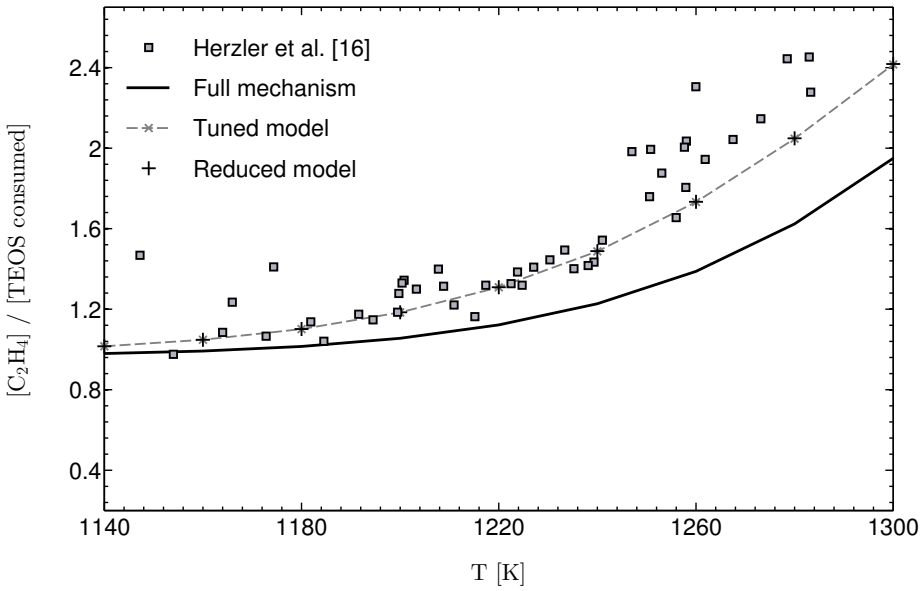

Figure 4: *Yield of ethylene as a fraction of decomposed TEOS.*

not only to TEOS, TREOS, DEOS and EOS, but also to every silica intermediate that can react in the same way. Since, the reaction rate coefficients for these channels are unknown, it was decided to approximate them. The activation energies were assumed to be equal to the reactions' endothermicities (see Table 3) and pre-exponential factors were set to 10^{16}, which can be thought of as an upper bound for the unimolecular process. Subsequently, the decomposition of diethyl ether was added with the rate constant coefficient taken from the study of Laidler and McKenney [22]. The additinal ethanol channels required 27 new

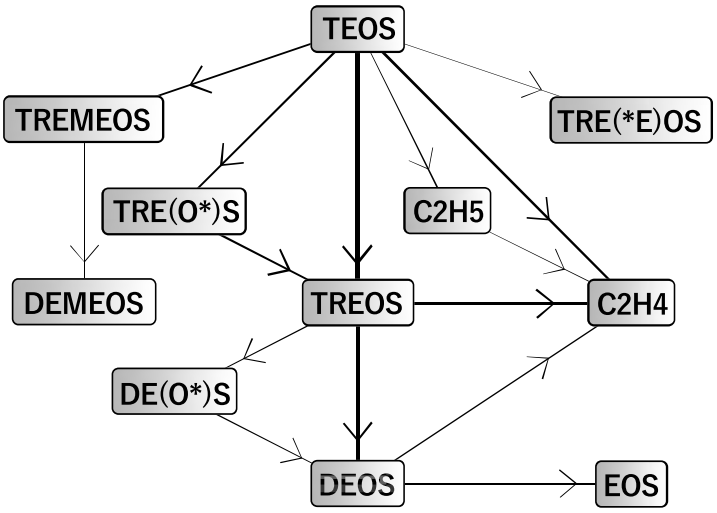

Figure 5: *The main TEOS decomposition channels at 1260 K. The arrows indicate the magnitude of the element C flux between species.*

O=Si(X)(Y) silica species, for which thermodynamic properties were estimated using methods described by Buerger et al. [5].

It was shown that the additional reactions were not sufficient to correctly reproduce the measured ethanol yield. Our model predictions were too low at almost all studied temperatures (T<1260 K) compared to the experimental measurements, even though the assumed rate constants are most likely much higher than the real unknown values. It was found that by reducing their activation energies by 10 kcal/mol good agreement could be reached. However, by doing so the total decomposition rate of TEOS is much higher than the uncertainties in the measurements by Herzler et al. [16] and our computations. Therefore, it is plausible that ethanol is mainly formed in a secondary step rather than directly from TEOS.

The mechanism responsible for the production of ethanol, unfortunately, still remains an open question. Reactions accounting for its formation used in our test study do not have known rate coefficients. We showed that even if these rates are approximated as an upper bound of the unimolecular process the ethanol is still not correctly reproduced (its yield is too low). Because of that and the fact that these rates will be most likely much much slower due to their high endothermicities and the fact that these reactions go through a transition state which would further increase their energy barriers we decided not to include them in the final TEOS mechanism used in further computations. However, the mentioned reactions are still provided as a comment in the detailed mechanism in the supplementary material.

3.3 Skeletal mechanism

The tuned mechanism from the previous section was used as a basis for the reduction. Figure 6 shows the sum of calculated RMS errors, $\bar{\varepsilon}_k$ for the first five target species,

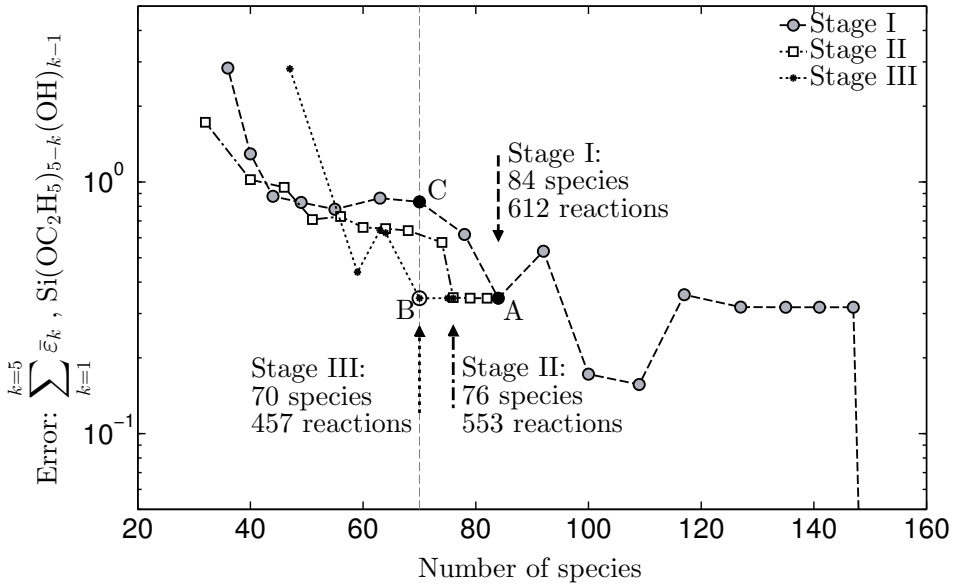

Figure 6: *Sum of the RMS errors of the first five targets as a function of the number of species in the model. Vertical line marks final mechanism size. Points A, B and C indicate the three skeletal mechanisms that were chosen for comparison.*

$Si(OC_2H_5)_{5-k}(OH)_k$, where $k \in [1..5]$, versus the number of retained species. After stage I, the mechanism was reduced to 84 species and 612 reactions having the cumulative error equal to 33% (with RMS error on individual targets below 15%). Further reduction in stage II eliminated 8 species and 59 corresponding reactions. After crossing this point, the errors rapidly increase (this can also be observed on the remaining Figures: 7-8, and 10-12), hence the choice of the mechanism size at each stage. Subsequent rate of progress analysis performed in stage III allowed the identification of 96 reactions and 6 species, whose removal do not significantly affect the error from stage II. The final choice of the mechanism size is indicated by the dashed vertical line shown each of Figure 6-12 and Figure 12. Points A, B, and C denote three different reduced mechanisms that were compared with the reference mechanism as per Figure 13. The point A is the mechanism obtained after stage I, point B indicates the mechanism after stage III, whereas point C is the mechanism having the same number of species as B, but obtained using a single-step reduction process.

Figures 7-12 depict the computed errors for the remaining target species (C_2H_4, O_2, and H_2) and on the temperature and the concentration of OH and H radicals. A similar trend as in Figure 6 can be observed, where the errors increase with the number of removed species. However, it is not strictly growing behaviour due to the fact that the importance coefficients from DRGEP are only the coarse representation of the actual elimination error. In all cases the errors for the chosen final mechanism are in the 1-15% range.

The normalized rates of progress of every reaction across all cases, Ω_i, are depicted in Figure 13. Most of these parameters are concentrated at the top of the plot ($10^{-9} - 10^0$ range). However, there are several reactions having rates of progress much below this region. In stage III of the reduction, a set of different thresholds was applied to remove

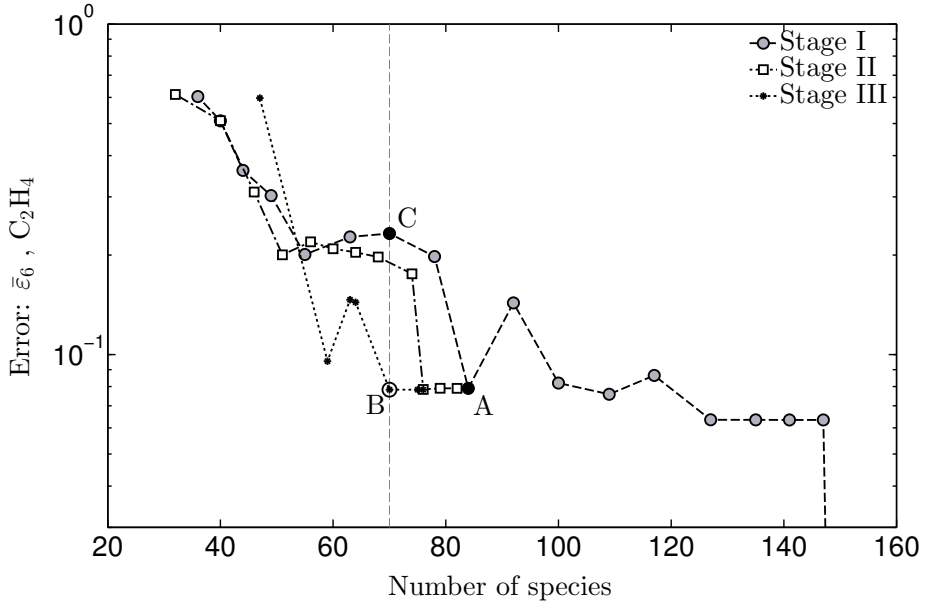

Figure 7: *A root mean square error in the C_2H_4 mole fraction as a function of the number of species in the model. Points A, B and C indicate the three skeletal mechanisms that were chosen for the comparison.*

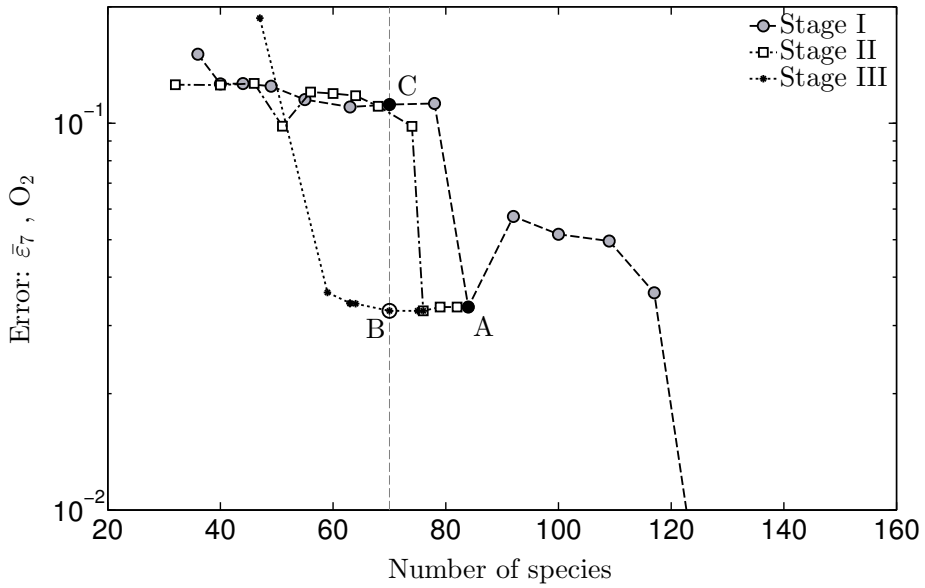

Figure 8: *A root mean square error in the O_2 mole fraction as a function of the number of species in the model. Points A, B and C indicate the three skeletal mechanisms that were chosen for the comparison.*

slow reactions. The dashed horizontal line shows the final choice of threshold, which results in the removal of 96 reactions and 6 species.

The dependence of the number of reactions on the number of species in the mechanism is

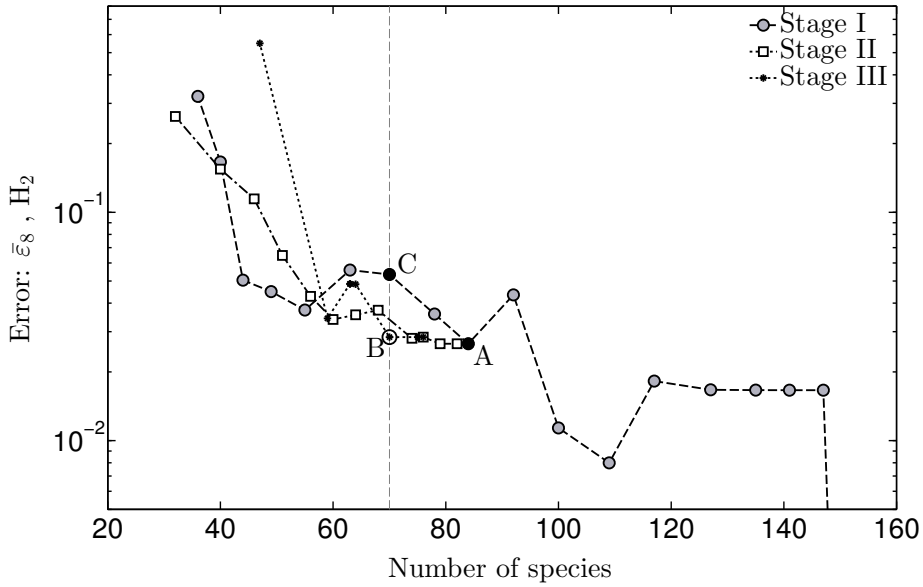

Figure 9: *A root mean square error in the H_2 mole fraction as a function of the number of species in the model. Points A, B and C indicate the three skeletal mechanisms that were chosen for the comparison.*

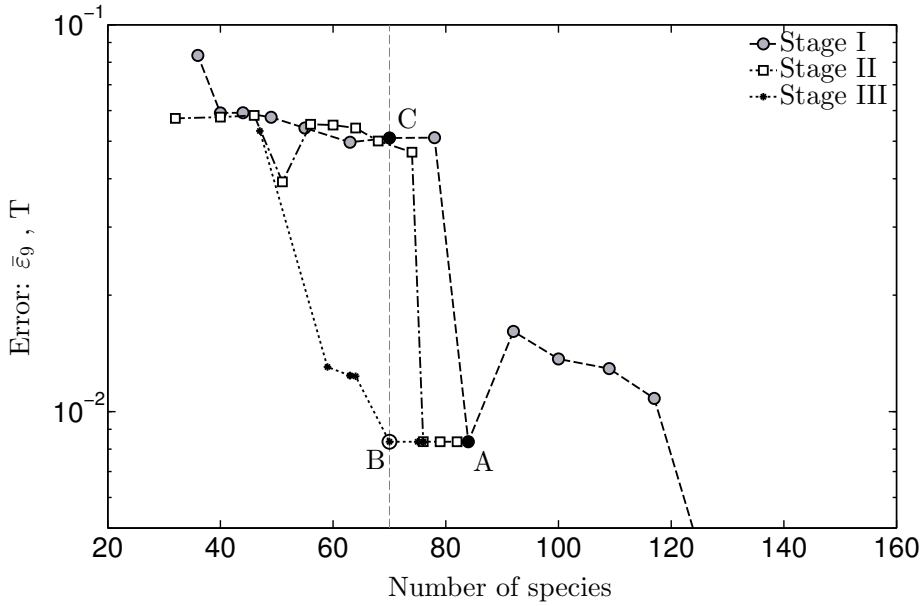

Figure 10: *A root mean square error in the temperature as a function of the number of species in the model. Points A, B and C indicate the three skeletal mechanisms that were chosen for the comparison.*

shown in Figure 14. It can be approximated as a linear relationship, having a coefficient of determination equal to $R^2 = 0.9905$. On average, removal of one species causes elimination of 13 reactions. The inset provides some insight into how the reduction in stage III proceeded. Firstly, reactions were removed by applying different thresholds on Ω_i. Sec-

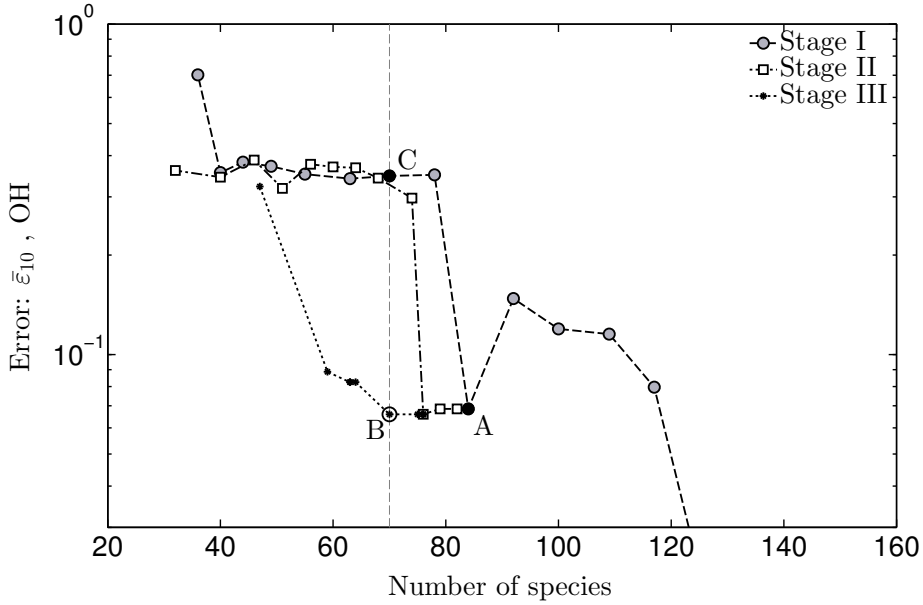

Figure 11: *A root mean square error in the OH mole fraction as a function of the number of species in the model. Points A, B and C indicate the three skeletal mechanisms that were chosen for the comparison.*

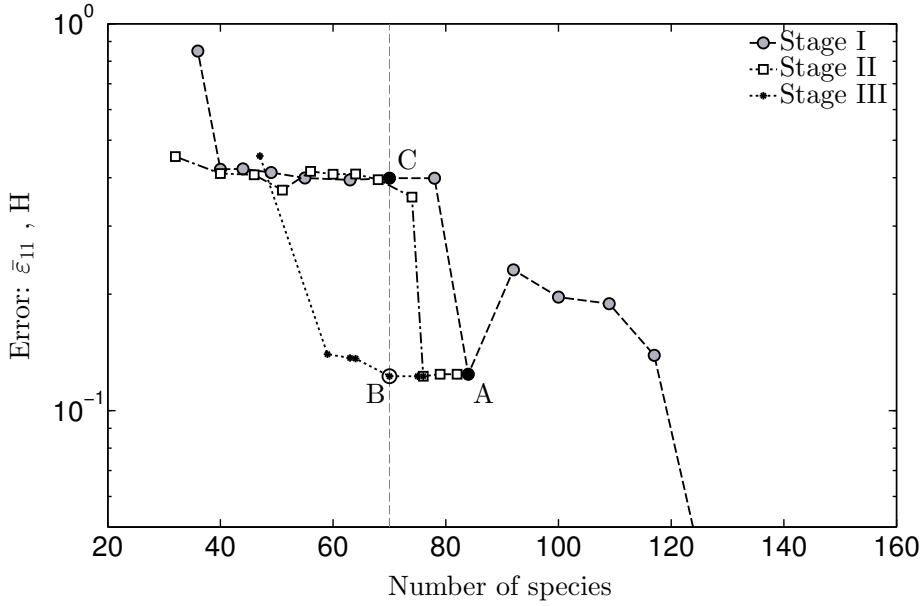

Figure 12: *A root mean square error in the H mole fraction as a function of the number of species in the model. Points A, B and C indicate the three skeletal mechanisms that were chosen for the comparison.*

ondly, if the removal of reactions caused a situation where there exist species that do not participate in any of the remaining channels, these species were removed as well. Therefore, in stage III two trends can be observed, where either number of reactions decreases keeping number of species constant or both decrease simultaneously.

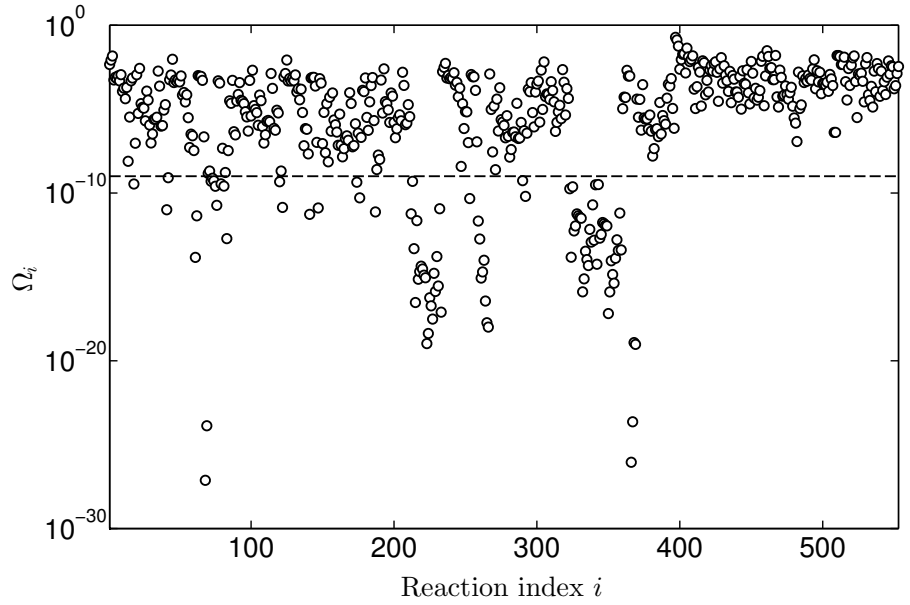

Figure 13: *Normalized rate of progress of each reaction after stage II reduction across all the cases. All reactions with Ω_i value lying below dashed horizontal line were removed from the final mechanism.*

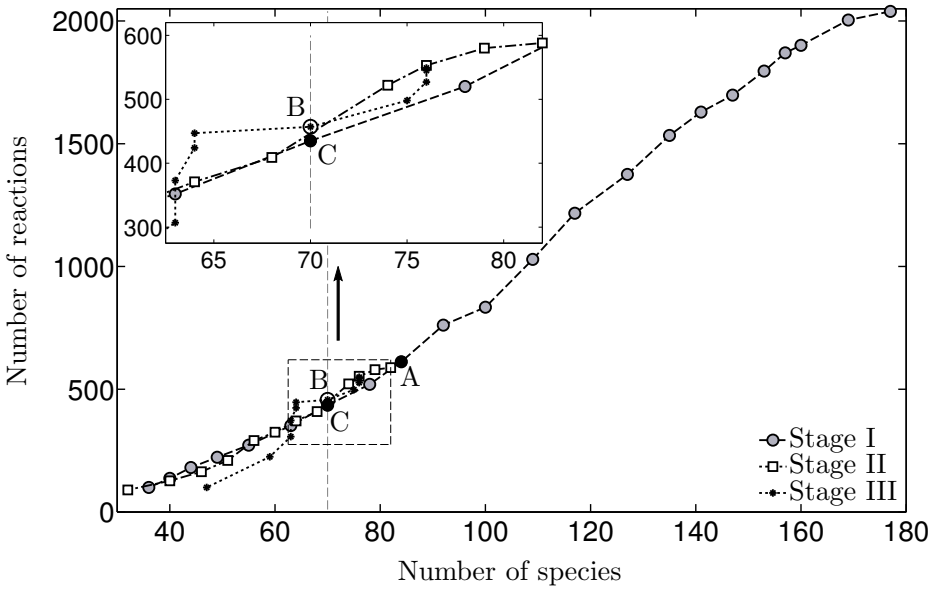

Figure 14: *Dependence of the number of reactions on the number of retained species. Points A, B and C indicate the three skeletal mechanisms that were chosen for the comparison.*

Figure 15 shows comparison between model predictions using the reference mechanism and corresponding predictions using mechanisms A, B and C for simulation case 29 in Table 2. The plots in the first and second rows compare the mole fractions of the target species. The plots in the third and fourth rows compare the mole fractions of OH and H

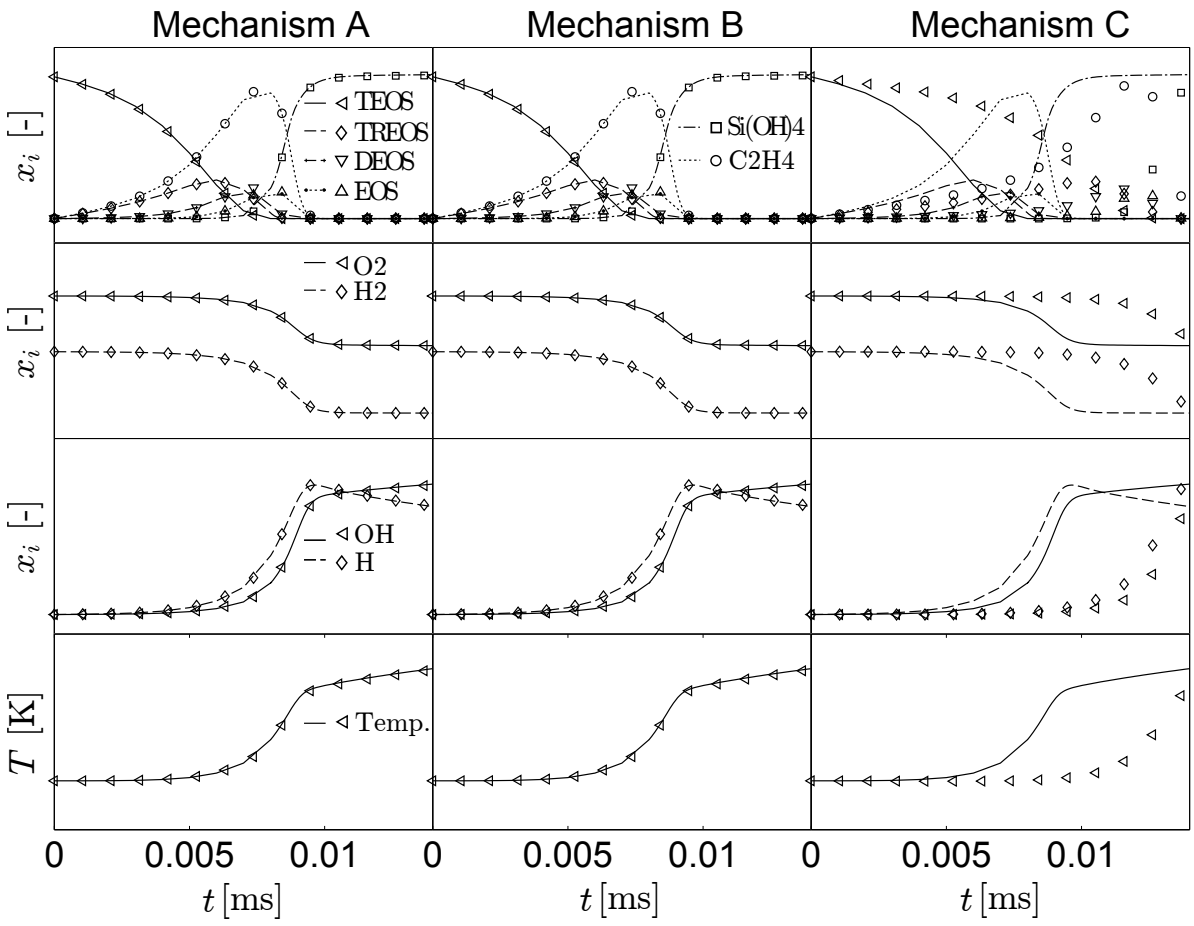

Figure 15: *Comparison of the three different skeletal models: A, B and C with the reference mechanism. Lines are the targets' data from the full model, while markers are data from the selected reduced models. Simulation conditions taken from case 29 in Table 2.*

radicals and temperature. The results from mechanisms A and B are virtually the same with respect to the selected targets. In both cases, very good agreement with the reference mechanism was obtained. The performance of the mechanism C is much worse. It can be explained by the fact that, although the number of species is the same for B and C, the set of species itself is different as is the number of reactions.

The difference between mechanisms B and C highlights benefits of a multistage reduction method. In case B the mechanism was built using a three-stage process, where the couplings between species were recomputed after stage I, taking into account the fact that a large number of species have already been eliminated. This modified the species priority order, which is why the set of species in B and C is not the same. Subsequently, stage III was applied to investigate the removal of slow reaction channels. These reactions were removed one by one, additionally checking if their reactants still participate in the mechanism via any other channel. If not, they were removed as well. The reason why it was possible to further remove the species without a significant increase in errors versus stages I and II, lies in the type of coupling between the removed species and the target species.

The species found in stage III (up to point B) do not have a strong *direct* connection with the targets, although they may be strongly and directly coupled with the remaining species via slow reactions. The final importance of the species in stage III to the targets depends then on the number and importance of the species that connect them. However, even if this importance is found to be high, the removal of the stage III-species is a secondary, tertiary or even higher order effect (depending on the length of the path that links them with the target), thus possibly having small impact on the target. Therefore, the last stage of the reduction while looking for slow reactions also closely inspects the species priority list and provides a set of candidate species for elimination (which could lie high on the species list). This further explains why the set of species in mechanism B and C is different. The final decision whether or not to remove the species was made by calculating the actual errors with and without the species. Mechanism B was also used to reproduce the experimental data on Figure 4. As can be seen, very good agreement was obtained.

4 Conclusions

The TEOS oxidation mechanism proposed by Nurkowski et al. [36] was improved by refining the rate parameters of key reaction channels. The rate of the ethylene loss from TEOS, TREOS, DEOS and DMDEOS was computed using transition state theory, where a CBS-Q method was employed for accurate estimation of the reaction energetics. The rates of the ethylene loss from EOS and C−C bond cleavage reactions were taken from the literature [37].

The performance of the refined TEOS mechanism was compared with experimental measurements. Very good agreement was observed for the total decomposition rate of TEOS and DMDEOS, where the maximum difference between the model and experiment was less than 20%. This is a significant improvement over the initial model [36], where the maximum difference in TEOS total rate constant was as large as a factor of 7. The ethylene production from TEOS, though, was found to be under-predicted by 20-30% at temperatures above 1220 K. This might be explained by the combined effect of recalculating the barrier heights of the important reactions contributing to the ethylene release, differences in the experimental and modelling parameters (e.g. residence time) and the effect of any missing channels (e.g. ethanol-producing reactions).

In order to partially resolve the problem with under-prediction of the ethylene, a parameter tuning was performed where some of the rate coefficients were adjusted within the error bounds of the calculated parameters. It was found that by increasing the rate constant of ethylene loss from TREOS and DEOS by a factor of 2, a good agreement with experiment can be achieved.

A skeletal version of the TEOS oxidation mechanism was created by employing a three-stage reduction procedure. The first and second stages involved a DRGEP method, whereas the third stage prioritised reactions according to their normalized rates of progress. The investigated conditions were taken from experimental studies of TEOS oxidation in oxygen-hydrogen flames. It was found that the addition of the extra two reductions stages enabled a higher reduction versus a single-stage approach. The final skeletal mechanism consists of 70 species and 457 reactions and provides good reproduction of the key model proper-

ties across the chosen process conditions.

An attempt was also made to investigate the formation of ethanol during the TEOS decomposition. Reactions producing the alcohol via silicates were systematically added into the mechanism. The new channels required 27 new silica species, for which thermodynamic properties were estimated. It was found that these reactions are unable to account for the ethanol formation due to their high endothermicities. This analysis suggests that ethanol is most likely formed in a secondary step rather than directly from TEOS. More study, unfortunately, is still required to understand this process. For now, it remains an open question.

5 Supplementary Information

The full and reduced TEOS gas-phase mechanisms and corresponding thermodynamic properties are provided in CHEMKIN format. Additionally, 27 new O=Si(X)(Y) silica species needed for the ethanol production analysis are added to the same thermodynamic properties file. The geometries of the studied molecules can be provided on request. 

Acknowledgements

This project is partly funded by the National Research Foundation (NRF), Prime Minister's Office, Singapore under its Campus for Research Excellence and Technological Enterprise (CREATE) programme.

References

[1] A. Abdali, M. Fikri, H. Orthner, H. Wiggers, and C. Schulz. Ignition delay times of shock-heated tetraethoxysilane, hexamethyldisiloxane, and titanium tetraisopropoxide. *Chemical Physics Letters*, 61:54–58, 2014. doi:10.1016/j.cplett.2014.03.079.

[2] M. Adachi, K. Okuyama, N. Tohge, M. Shimada, J. Satoh, and M. Muroyama. Gas-phase nucleation in an atmospheric pressure chemical vapour deposition process for SiO_2 films using tetraethylorthosilicate (TEOS). *Japanese Journal of Applied Physics*, 31(2):1439–1442, 1992.

[3] J. Akroyd, A. J. Smith, R. Shirley, L. R. McGlashan, and M. Kraft. A coupled CFD-population balance approach for nanoparticle synthesis in turbulent reacting flows. *Chemical Engineering Science*, 66(17):3792–3805, 2011. doi:10.1016/j.jcp.2013.09.021.

[4] A. D. Becke. Density–functional thermochemistry. III. The role of exact exchange. *Journal of Chemical Physics*, 98(7):5648–5651, 1993. doi:10.1063/1.464913.

[5] P. Buerger, D. Nurkowski, J. Akroyd, S. Mosbach, and M. Kraft. First-Principles Thermochemistry for the Thermal Decomposition of Titanium Tetraisopropoxide. *Journal of Physical Chemistry A*, 119(30):8376–8387, 2015. doi:10.1021/acs.jpca.5b01721.

[6] J. C. S. Chu, J. Breslin, N. Wang, and M. C. Lin. Relative stabilities of tetramethyl orthosilicate and tetraethylorthosilicate in the gas phase. *Materials Letters*, 12:179–184, 1991. doi:10.1016/0167-577X(91)90170-B.

[7] J. C. Cramer. *Essentials of Computational Chemistry: Theories and Models 2nd Edition*. John Wiley & Sons, Ltd, 2004. ISBN 978-0-470-09182-1.

[8] L. A. Curtiss, K. Raghavachari, G. W. Trucks, and J. A. Pople. Gaussian-2 theory for molecular energies of first- and second-row compounds. *Journal of Chemical Physics*, 94:7221–7230, 1991. doi:10.1063/1.460205.

[9] B. Delperier, C. Vinante, and R. Moranche. Analysis and modelling of tetraethoxysilane pyrolysis. *Journal of Analytical and Applied Pyrolysis*, 13(1-2):141–149, 1988. doi:10.1016/0165-2370(88)80054-8.

[10] J. B. Foresman and Æ. Frish. *Exploring Chemistry with Electronic Structure Methods*. Gaussian; 2 edition, 1996. ISBN 978-0963676931.

[11] M. J. Frisch, G. W. Trucks, H. B. Schlegel, G. E. Scuseria, Robb, et al. Gaussian09 Revision D.01, 2009. Gaussian Inc. Wallingford CT 2009.

[12] K. Fukui. The Path of Chemical Reactions - The IRC Approach. *Accounts of Chemical Research*, 14:363–368, 1981. doi:10.1021/ar00072a001.

[13] P. George, M. Trachtman, A. M. Brett, and C. W. Bock. Comparison of Various Isodesmic and Homodesmotic Reaction Heats with Values derived from Published Ab initio Molecular Orbital Calculations. *Journal of the Chemical Society, Perkin Transactions 2*, (8):1036–1047, 1977. doi:10.1039/P29770001036.

[14] Y. Georgievskii, J. A. Miller, M. P. Burke, and S. J. Klippenstein. Reformulation and Solution of the Master Equation for Multiple-Well Chemical Reactions. *Journal of Physical Chemistry A*, 117(46):12146–12154, 2013. doi:10.1021/jp4060704.

[15] C. Hankwon, J. H. Park, and H. D. Jang. Flame synthesis of silica nanoparticles by adopting two-fluid nozzle spray. *Colloids and Surfaces A: Physicochemical and Engineering Aspects*, 313-314:140–144, 2008. doi:10.1016/j.colsurfa.2007.04.083.

[16] J. Herzler, J. A. Manion, and W. Tsang. Single–pulse shock tube study of the decomposition of tetraethoxysilane and related compounds. *Journal of Physical Chemistry A*, 101:5500–5508, 1997. doi:10.1021/jp9706543.

[17] P. Ho and C. F. Melius. Theoretical study of the thermochemistry of molecules in the Si-O-H-C system. *Journal of Physical Chemistry*, 99:2166–2176, 1995. doi:10.1021/j100007a056.

[18] H. D. Jang. Generation of silica nanoparticles from tetraethylorthosilicate (TEOS) vapor in a diffusion flame. *Aerosol Science and Technology*, 30(5):477–488, 1999. doi:10.1080/027868299304516.

[19] H. D. Jang. Experimental study of synthesis of silica nanoparticles by a bench-scale diffusion flame reactor. *Powder Technology*, 119(2-3):102–108, 2001. doi:10.1016/S0032-5910(00)00407-1.

[20] H. D. Jang, H. Chang, Y. Suh, and K. Okuyama. Synthesis of SiO_2 nanoparticles from sprayed droplets of tetraethylorthosilicate by the flame spray pyrolysis. *Current Applied Physics*, 6(1):e110–e113, 2006. doi:0.1016/j.cap.2006.01.021.

[21] L. S. Kassel. Studies in Homogeneous Gas Reactions. ii. Introduction of Quantum Theory. *Journal of Physical Chemistry*, 32(7):1065–1079, 1928. doi:10.1021/j150289a011.

[22] K. J. Laidler and D. J. McKenney. Kinetics and Mechanisms of the Pyrolysis of Diethyl Ether. II. the Reaction Inhibited by Nitric Oxide. *Royal Society Proceedings A*, 278(1375):517–526, 1964. doi:10.1098/rspa.1964.0080.

[23] C. Lee, W. Yang, and R. G. Parr. Development of the Colle-Salvetti correlation-energy formula into a functional of the electron density. *Physical review B*, 37(2): 785–789, 1988. doi:10.1103/PhysRevB.37.785.

[24] T. Løvås. *Automatic Reduction Procedures for Chemical Mechanisms in Reactive Systems*. PhD thesis, Lund University, 2002.

[25] T. Løvås, D. Nilsson, and F. Mauss. Automatic reduction procedure for chemical mechanisms applied to premixed methane/air flames. *Proceedings of the Combustion Institute*, 28(2):1809–1815, 2000. doi:10.1016/S0082-0784(00)80583-4.

[26] T. Løvås, P. Amnéus, F. Mauss, and E. Mastorakos. Comparison of automatic reduction procedures for ignition chemistry. *Proceedings of the Combustion Institute*, 29(1):1387–1393, 2002. doi:10.1016/S1540-7489(02)80170-5.

[27] T. Lu and C. K. Law. Directed relation graph method for mechanism reduction. *Proceedings of the Combustion Institute*, 30(1):1333–1341, 2005. doi:10.1016/j.proci.2004.08.145.

[28] T. Lu and C. K. Law. Linear time reduction of large kinetic mechanisms with directed relation graph: n-Heptane and iso-octane. *Combustion and Flame*, 144:24–36, 2006. doi:10.1016/j.combustflame.2005.02.015.

[29] R. A. Marcus. Statistical Theory of Unimolecular Reactions and Intramolecular Dynamics. *Laser Chemistry*, 2(5-6):203–217, 1983. doi:10.1155/LC.2.203.

[30] N. M. Marinov. A detailed chemical kinetic model for high temperature ethanol oxidation. *International Journal of Chemical Kinetics*, 31(3):183–220, 1999.

[31] W. J. Menz, J. Akroyd, and M. Kraft. Stochastic solution of population balance equations for reactor networks. *Journal of Computational Physics*, 256(1):615–629, 2014. doi:10.1016/j.jcp.2013.09.021.

[32] J. A. Montgomery, J. W. Ochterski, and G. A. Petersson. A complete basis set model chemistry. vi. use of density functional geometries and frequencies. *Journal of Chemical Physics*, 110(6):2822–2827, 1999. doi:10.1063/1.477924.

[33] S. Mosbach, S. Haiyun, and M. Kraft. A new algorithm for the direct simulation of combustion systems and its application to reaction elimination. *Proceedings of the Combustion Institute*, 30(1):1301–1308, 2005. doi:10.1016/j.proci.2004.08.115.

[34] K. E. Niemeyer and C.-J. Sung. On the importance of graph search algorithms for DRGEP-based mechanism reduction methods. *Combustion and Flame*, 158(8): 1439–1443, 2011. doi:10.1016/j.combustflame.2010.12.010.

[35] D. Nilsson. *Automatic Analysis and Reduction of Reaction Mechanisms for Complex Fuel Combustion*. PhD thesis, Lund University, 2001.

[36] D. Nurkowski, P. Buerger, J. Akroyd, and M. Kraft. A detailed kinetic study of the thermal decomposition of tetraethoxysilane. *Proceedings of the Combustion Institute*, 35(2):2291–2298, 2015. doi:10.1016/j.proci.2014.06.093.

[37] D. Nurkowski, S. J. Klippenstein, Y. Georgievskii, M. Verdicchio, A. W. Jasper, J. Akroyd, S. Mosbach, and M. Kraft. Ab initio Variational Transition State Theory and Master Equation Study of the Reaction $(OH)_3SiOCH_2 + CH_3 \rightleftharpoons (OH)_3SiOC_2H_5$. *Zeitschrift für Physikalische Chemie*, 334:1–18, 2015. doi:10.1515/zpch-2014-0640.

[38] J. W. Ochterski and J. A. Montgomery. A complete basis set model chemistry. v. extensions to six or more heavy atoms. *Journal of Chemical Physics*, 104(7):2598–2619, 1996. doi:10.1063/1.470985.

[39] J. Park, R. S. Zhu, and M. C. Lin. Thermal decomposition of ethanol. i. Ab initio molecular orbital/Rice-Ramsperger-Kassel-Marcus prediction of rate constant and product branching ratios. *Journal of Chemical Physics*, 117, 2002. doi:10.1063/1.1490601.

[40] P. Pepiot-Desjardins and H. Pitsch. An efficient error-propagation-based reduction method for large chemical kinetic mechanisms. *Combustion and Flame*, 154(1-2): 67–81, 2008. doi:10.1016/j.combustflame.2007.10.020.

[41] W. Phadungsukanan, S. Shekar, R. Shirley, M. Sander, R. H. West, and M. Kraft. First-principles thermochemistry for silicon species in the decomposition of tetraethoxysilane. *Journal of Physical Chemistry A*, 113:9041–9049, 2009. doi:10.1021/jp905494s.

[42] O. K. Rice and H. C. Ramsperger. Theories of unimolecular gas reactions at low pressures. *Jorunal of the American Chemical Society*, 49(7):1617–1629, 1927. doi:10.1021/ja01406a001.

[43] M. Sander, R. H. West, M. S. Celnik, and M. Kraft. A Detailed Model for the Sintering of Polydispersed Nanoparticle Agglomerates. *Aerosol Science and Technology*, 43(10):978–989, 2009. doi:10.1080/02786820903092416.

[44] S. Shekar, W. J. Menz, A. J. Smith, M. Kraft, and W. Wagner. On a multivariate population balance model to describe the structure and composition of silica nanoparticles. *Computers and Chemical Engineering*, 43(10):130–147, 2012. doi:10.1016/j.compchemeng.2012.04.010.

[45] S. Shekar, M. Sander, R. C. Riehl, A. J. Smith, A. Braumann, and M. Kraft. Modelling the flame synthesis of silica nanoparticles from tetraethoxysilane. *Chemical Engineering Science*, 70(5):54–66, 2012. doi:10.1016/j.ces.2011.06.010.

[46] R. Shirley, Y. Liu, T. S. Totton, R. H. West, and M. Kraft. First-Principles Thermochemistry for the Combustion of a TiCl4 and AlCl3 Mixture. *Journal of Physical Chemistry A*, 113(49):13790–13796, 2009. doi:10.1021/jp905244w.

[47] R. Sivaramakrishnan, M. C. Su, J. V. Michael, S. J. Klippenstein, L. B. Harding, and B. Ruscic. Rate Constants for the Thermal Decomposition of Ethanol and Its Bimolecular Reactions with OH and D: Reflected Shock Tube and Theoretical Studies. *Journal of Physical Chemistry A*, 114(35):9425–9439, 2010. doi:10.1021/jp104759d.

[48] J. Smolik and P. Moravec. Gas phase synthesis of fine silica particles by oxidation of tetraethylorthosilicate vapour. *Journal of Materials Science Letters*, 14(6):387–389, 1995. doi:10.1007/BF00274548.

[49] L. C. Snyder. Heats of Reaction from Hartree-Fock Energies of Closed-Shell Molecules. *Journal of Chemical Physics*, 46(9):3602–3602, 1967. doi:10.1063/1.1841264.

[50] H. S. Soyhan, F. Mauss, and C. Sorusbay. Chemical kinetic modeling of combustion in internal combustion engines using reduced chemistry. *Combustion Science and Technology*, 174(11-12):73–91, 2010. doi:10.1080/713712950.

[51] A. S. Tomlin, T. Turányi, and M. J. Pilling. Chapter 4 Mathematical tools for the construction, investigation and reduction of combustion mechanisms; in: M. J. Pilling (Editor) Low-Temperature Combustion and Autoignition. *Comprehensive Chemical Kinetics*, 35:293–437, 1997. doi:10.1016/S0069-8040(97)80019-2.

[52] A. S. Tomlin, T. Turányi, and S. Alison. *Analysis of Kinetic Reaction Mechanisms*. Springer-Verlag Berlin Heidelberg, 2014. ISBN 978-3-662-44562-4.

[53] R. H. West, G. J. O. Beran, W. H. Green, and M. Kraft. First-Principles Thermochemistry for the Production of TiO_2 from $TiCl_4$. *Journal of Physical Chemistry A*, 111(18):3560–3565, 2007. doi:10.1021/jp0661950.